ACS Catalysis

pubs.acs.org/acscatalysis

Research Article

Mechanism of Cobalt-Catalyzed Direct Aminocarbonylation of Unactivated Alkyl Electrophiles: Outer-Sphere Amine Substitution To Form Amide Bond

Jiandong Guo, Hai D. Pham, Yan-Bo Wu, Dongju Zhang, and Xiaotai Wang*

Cite This: *ACS Catal.* 2020, 10, 1520−1527

Read Online

ACCESS | Metrics & More | Article Recommendations | Supporting Information

ABSTRACT: Experimentalists have recently achieved the first chemoselective aminocarbonylation of unactivated alkyl electrophiles, using the common cobalt reagent $Co_2(CO)_8$ as a catalyst. Here, we present a detailed density functional theory (DFT) mechanistic study on this remarkable reaction. Induced by the Lewis base morpholine (or MOR, the amine substrate), $Co_2(CO)_8$ disproportionates to $[Co(CO)_3(MOR)_2]^+$ and $[Co(CO)_4]^-$. The active catalyst $[Co(CO)_4]^-$ undergoes an S_N2 reaction with the alkyl tosylate substrate to form an alkylcobalt(I) carbonyl intermediate with an inverted configuration at the α-carbon. The alkylcobalt(I) carbonyl complex favors CO migratory insertion over β-hydride elimination. The resulting acylcobalt(I) carbonyl intermediate, along with the MOR and CO substrates, could introduce several pathways for the amide C−N bond formation. The inner-sphere pathways involving Co(I)-bound MOR are ruled out. The outer-sphere pathway in which MOR attacks the Co(I)-bound acyl leads to the amide product and the regenerated $[Co(CO)_4]^-$. The S_N2 process is the rate-determining step with the largest energy span ($\Delta G^{\ddagger}$ = 22.8 kcal/mol). The side reaction of double CO insertion faces a higher selectivity-determining energy barrier and hence is less favorable. This DFT work provides deep mechanistic insights into the $Co_2(CO)_8$-promoted chemoselective aminocarbonylation of unactivated alkyl electrophiles, thereby having implications for organocobalt catalysis and transition-metal-catalyzed amide C−N bond-forming reactions.

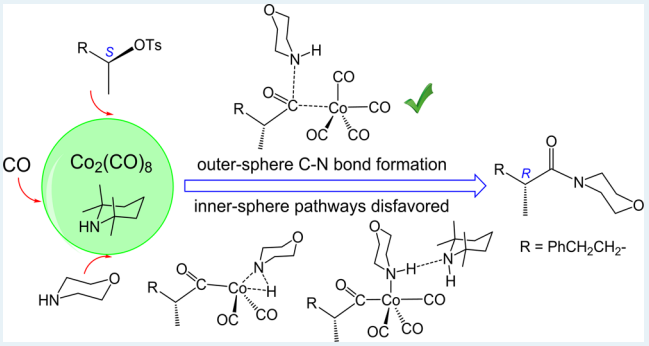

KEYWORDS: *cobalt catalysis, $Co_2(CO)_8$, aminocarbonylation, outer-sphere mechanism, amide C−N bond formation*

1. INTRODUCTION

The amide functionality is a common structural motif in organic compounds, including many bioactive natural products and pharmaceutical agents. Organic amides are traditionally synthesized by coupling carboxylic acids and amines.[1] As first reported by Schoenberg and Heck,[2] palladium-catalyzed direct, three-component aminocarbonylation provides a concise and efficient approach to amides, using aryl electrophiles (halides/pseudohalides), amines, and carbon monoxide (CO) as substrates.[3] The active catalyst is thought to be a Pd(0) complex, which reacts with an aryl halide/pseudohalide substrate by concerted oxidative addition to start the catalytic cycle. This aminocarbonylation protocol, however, does not work well for alkyl electrophiles. There were only a few reported procedures involving the use of alkyl iodides, and these reactions were thought to proceed by a radical mechanism, typically required high-energy irradiation and frequently yielded a greater amount of undesired byproducts from double CO insertion.[4] Alexanian and Sargent have recently made a breakthrough and reported a cobalt-catalyzed aminocarbonylation of unactivated alkyl tosylates, as shown by the representative reaction in Scheme 1.[5] This method makes use of a common, commercially available cobalt reagent, $Co_2(CO)_8$, as a catalyst and delivers the amide product chemoselectively, thereby providing the first practical aminocarbonylation protocol for unactivated alkyl electrophiles. Obviously, the mode of reactivity of cobalt, which differs from that of palladium, enables the catalytic reaction.

Scheme 1. Direct Aminocarbonylation of C(sp^3)-Electrophiles via Cobalt Catalysis

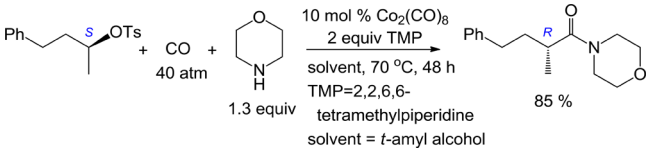

Received: November 2, 2019
Revised: December 22, 2019
Published: December 23, 2019

Alexanian and Sargent proposed a brief catalytic cycle, as shown in Figure 1. Lewis base-induced disproportionation of

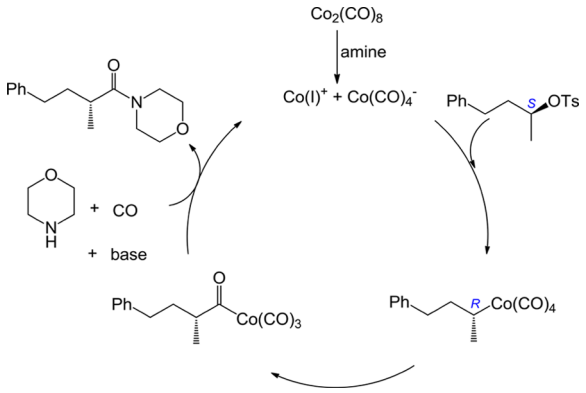

Figure 1. Proposed catalytic cycle for the Co-catalyzed aminocarbonylation.

$Co_2(CO)_8$ yields $[Co(CO)_4]^-$, which displaces the tosylate group by the S_N2 mechanism, forming a Co(I) alkyl intermediate with an inverted configuration at the α-carbon. The S_N2-associated Walden inversion is responsible for the stereospecificity of the reaction. The Co(I) alkyl intermediate converts into a Co(I) acyl species through CO migratory insertion. A formal nucleophilic displacement of the carbonylcobalt moiety with morpholine delivers the amide product and regenerates the active catalyst $[Co(CO)_4]^-$.

The intriguing questions about this novel catalytic reaction inspired our interest. How is the active catalyst initiated from the cobalt reagent $Co_2(CO)_8$? Why does the Co(I) alkyl intermediate favor CO migration over β-hydride elimination? To what extent does double CO insertion occur from the Co(I) acyl intermediate? Is the amide C–N bond in the product formed by an inner-sphere mechanism involving amine coordination to cobalt or through an outer-sphere pathway? What is the rate-determining step?

In this DFT computational study, we address these questions in the context of relevant organotransition metal reactivity and catalysis. We aim to establish a detailed and plausible mechanism that would not only elucidate the title reaction but may also provide useful insights into understanding and improving transition-metal-catalyzed amide bond-forming reactions in general.

2. COMPUTATIONAL METHODS

All calculations were performed with Gaussian 09.[6] The hybrid functional B3LYP[7] was combined with the dispersion correction D3[8] to improve computational accuracy. Geometries are optimized and characterized by frequency calculations to be energy minima (zero imaginary frequencies) or transition states (only one imaginary frequency) at the B3LYP-D3/BS1 level in the gas phase, BS1 designating a mixed basis set of SDD[9] for cobalt and 6-31G(d,p) for other atoms. The energies were then refined by B3LYP-D3/BS2//B3LYP-D3/BS1 single-point energy calculations in *t*-butyl alcohol, using the SMD solvation model,[10,11] BS2 denoting a mixed basis set of SDD for cobalt and 6-311++G(d,p) for other atoms. The refined energies were converted to zero-point energy-corrected free energies at 298.15 K and 1 atm, using the B3LYP-D3/BS1 harmonic frequencies. Corrections were then made to the free energies on the basis of "the theory of free volume", that is, for 2-to-1 (or 1-to-2) reactions, a correction of −2.6 (or 2.6) kcal/mol was applied.[12] For comparison purposes, the key energy minima and transition states were reoptimized in solution using the SMD solvation model, and the results were consistent with those obtained with gas-phase optimizations (Figure S1).

3. RESULTS AND DISCUSSION

3.1. Precatalyst Initiation. Dicobalt octacarbonyl, $Co_2(CO)_8$, has received much attention over the years because it acts as a catalyst or precatalyst for hydroformylation (the classical oxo process),[13] Pauson–Khand [2 + 2 + 1] cycloaddition,[14] and other reactions.[15] Previous studies have established that in solution, $Co_2(CO)_8$ adopts an equilibrium mixture of three isomeric forms,[16] with the D_{2d} symmetry structure being proposed as the lowest energy isomer.[17] Our calculations are consistent with these earlier findings, showing **1cat** as the zero of energy and only small differences in energy between the three isomers (Figure 2).

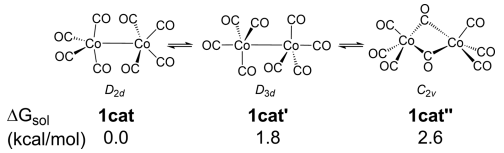

Figure 2. Computed structures and relative energies of three isomers of $Co_2(CO)_8$.

It is known that under the influence of a Lewis base (L), $Co_2(CO)_8$ can disproportionate to 18-electron $[CoL_n(CO)_{5-n}]^+$ and $[Co(CO)_4]^-$,[18] but there have been no reports of computational studies on the process. In the current reaction system, L would be 2,2,6,6-tetramethylpiperidine (TMP) or morpholine (MOR), both of which are present in excess quantities. We optimized five complexes of the $[CoL_n(CO)_{5-n}]^+$ type (L = TMP or MOR) and evaluated the free energies of their formation reactions, as shown in Table 1. Reaction 2 has the most favorable thermodynamics (ΔG = −4.4 kcal/mol) among the five reactions.

We computed the pathway of reaction 2 to gain mechanistic insight into the precatalyst initiation. As shown in Figure 3, the van der Waals complex **IM1** orients the N donor atom of MOR toward Co^1 although there is no bonding interaction between them and essentially no change in the Co^1–Co^2 bond distance. The N···Co^1 distance (3.55 Å) is equal to the sum of the van der Waals radii of N (1.55 Å)[19] and Co (2.0 Å),[20] suggesting an optimal van der Waals contact. There are several other such van der Waals contacts between the atoms of the two fragments of **IM1** (Figure S3). As MOR approaches Co^1, the transition state **TS1** is reached where a Co^1–N bond is partially formed at 2.70 Å, the Co^1–Co^2 bond is largely broken at 3.13 Å, and a Co^1-bound CO ligand shifts toward a μ^2 mode to bridge the Co^2 atom. **TS1** proceeds to the dinuclear complex **IM2**, where the Co^2–C(bridging) bond at 2.17 Å is longer than the Co^1–C(bridging) bond at 1.99 Å. A natural bond orbital analysis of **IM2** assigns Wiberg bond indices (WBI) 0.78 and 0.61 for the Co^1–C(bridging) and Co^2–C(bridging) bonds, respectively. The two sets of data taken together, namely, bond distances and WBI, indicate that the Co^2–C(bridging) connectivity in **IM2** is a bond although it is significantly weaker than the Co^1–C(bridging) bond. The heterolysis of **IM2** along the Co^2–C(bridging) bond is

https://dx.doi.org/10.1021/acscatal.9b04736
ACS Catal. 2020, 10, 1520–1527

Table 1. Free-Energy Changes (kcal/mol) for Precatalyst Initiation[a]

reaction	ΔG
(1) $Co_2(CO)_8$ + MOR → $[Co(CO)_4(MOR)]^+$ + $[Co(CO)_4]^-$	2.8
(2) $Co_2(CO)_8$ + 2MOR → $[Co(CO)_3(MOR)_2]^+$ + $[Co(CO)_4]^-$ + CO	−4.4
(3) $Co_2(CO)_8$ + TMP → $[Co(CO)_4(TMP)]^+$ + $[Co(CO)_4]^-$	2.1
(4) $Co_2(CO)_8$ + 2TMP → $[Co(CO)_3(TMP)_2]^+$ + $[Co(CO)_4]^-$ + CO	1.1
(5) $Co_2(CO)_8$ + MOR + TMP → $[Co(CO)_3(MOR)(TMP)]^+$ + $[Co(CO)_4]^-$ + CO	−3.6

[a]The spin triplets of the five Co(I) complex cations are lower in energy than the singlets and hence are used for ΔG calculations (see Figure S2).

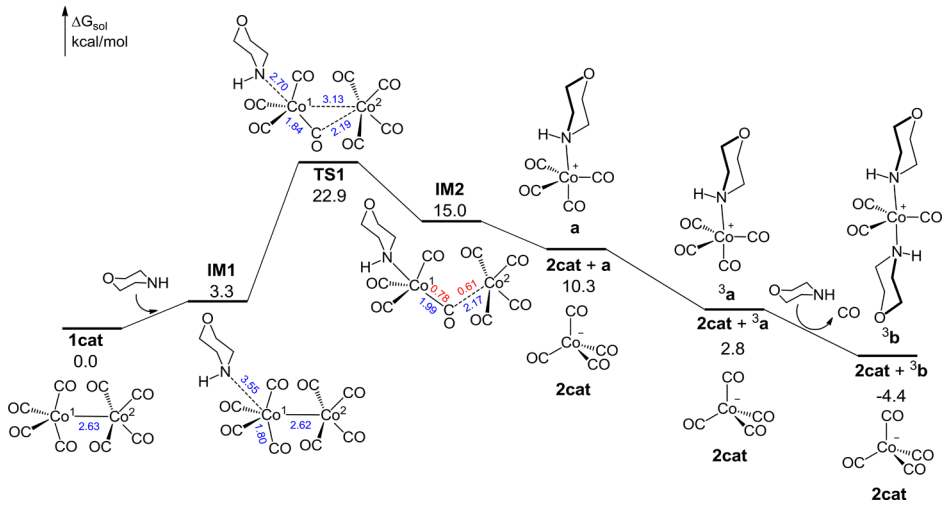

Figure 3. Free-energy profile for the pathway of precatalyst initiation. Selected bond distances in blue font are given in Å (the same below). The numbers shown in red font on selected bonds in **IM2** denote the Wiberg bond indices. The left superscript 3 on **a**/**b** indicates the spin triplet state.

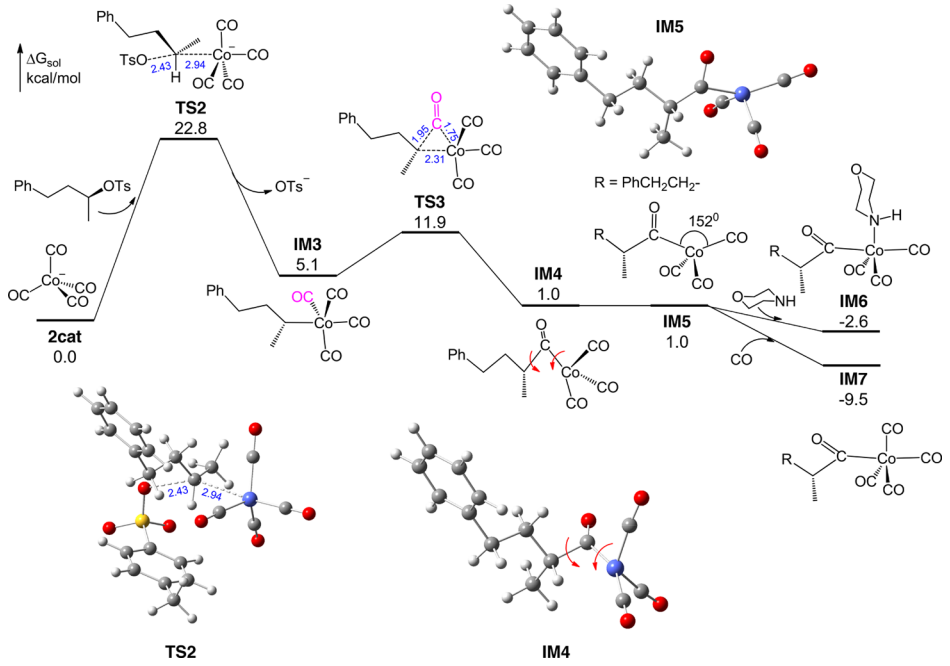

Figure 4. Free-energy profile for the S_N2 step, CO migratory insertion, and MOR/CO coordination. **2cat** is taken as the new zero reference level of energy after the exergonic initiation.

exergonic, giving the active catalyst $[Co(CO)_4]^-$ (**2cat**). The resulting complex cation $[Co(CO)_4(MOR)]^+$ (**a**) changes to the more stable triplet ^{3}**a**, which undergoes exergonic substitution of MOR for CO to form the triplet complex ^{3}**b**. In summary, our results reveal a detailed mechanism for Lewis base-induced disproportionation of $Co_2(CO)_8$. It occurs via indirect heterolytic Co−Co bond cleavage, that is, by electron transfer through a bridging CO ligand.

3.2. S_N2 Reaction and CO Insertion. $[Co(CO)_4]^-$ (**2cat**) is a modest nucleophile known to react with alkyl tosylates by an S_N2 process to generate alkylcobalt carbonyl complexes.[21] This led us to trace the S_N2 transition state **TS2**, which releases

https://dx.doi.org/10.1021/acscatal.9b04736
ACS Catal. 2020, 10, 1520−1527

the tosylate anion and proceeds to the Co(I) alkyl complex **IM3** (Figure 4). **TS2** is 22.8 kcal/mol relative to **2cat**, a reasonable energy barrier for the reaction conditions. In **IM3**, three CO ligands are of cis geometry to the Co−C(alkyl) bond, which has free rotation, and by considering different conformations from this bond rotation, we found **TS3** to be the lowest energy barrier for the carbonyl migratory insertion into the Co−C(alkyl) bond, which is 11.9 kcal/mol relative to **2cat**. Thus, the carbonyl insertion step would be facile, leading to the four-coordinate 16-electron Co(I) acyl complex **IM4**. **IM4** has a conformation where the large acyl group would hinder substrate coordination to the vacant metal site. This can be resolved by the indicated rotations about the single bonds to give the isoenergetic conformer **IM5** with an open space around the fifth metal coordination site, which can be occupied by MOR or CO to form the 18-electron complex **IM6** or **IM7**.

We also considered the nucleophilic attack of MOR on a CO ligand of **IM3** to form an alkylcarbamylcobalt(I) complex that could yield the amide product via intramolecular alkyl migration. This mechanism, however, is disfavored because the alkylcarbamylcobalt(I)-forming transition states are higher in energy than **TS3** by at least 5.6 kcal/mol (Figure S4).

3.3. Amide Formation and Catalyst Regeneration. We first considered possible inner-sphere pathways through **IM6**. Examination of the cis geometric relationship between the MOR and acyl ligands in **IM6** suggests a likely oxidative addition (OA) of the MOR N−H bond to the Co(I) center to form an acylcobalt(III) amido complex, which can undertake acyl−amido reductive elimination/coupling to deliver the product. We traced the OA transition state **TS4**, which is 58.6 kcal/mol with respect to **IM6** (Figure 5). This energy

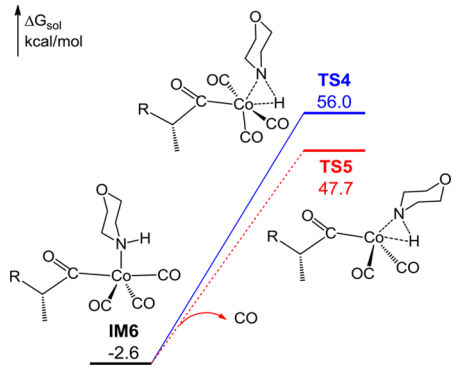

Figure 5. Transition states of N−H bond oxidative addition to Co(I).

barrier would be too high to be crossed by the reaction. Dissociation of one CO ligand from **IM6** can lower the barrier to **TS5**, but it would still be too high to be reached.

Previous studies have suggested that the N−H bond oxidative addition to 4d or 5d late transition-metal complexes tends to have a high activation energy, with barriers of 41.0−51.2 kcal/mol calculated for some Ir(I) and Rh(I) complexes.[22] A plausible explanation invokes the repulsive, destabilizing effect of M ← N(amido) π-donation on the M−N(amido) bond, where M is a late transition metal with five or more valence d electrons.[23] It follows from this rationale that the N−H bond oxidative addition to the 3d Co(I) complex **IM6** would face even higher energy barriers because of the stronger repulsion arising from the smaller size of Co(I). Therefore, the calculated barriers shown in Figure 5 are understandable.

In the Buchwald−Hartwig amination mechanism, the Pd(II)-coordinated amine substrate is deprotonated by a base additive.[24] Mechanistic studies on some palladium-catalyzed aminocarbonylations of aryl halides suggest a similar inner-sphere mechanism, wherein the Pd(II)-coordinated amine substrate is deprotonated to form an acylpalladium(II) amido species, which undergoes acyl−amido reductive elimination to generate the amide product.[25] Therefore, we considered TMP, the base additive in the current reaction system, for deprotonating the N−H bond of the Co(I)-bound MOR in **IM6**. Four **IM6**−TMP complexes with various TMP dispositions were optimized, but no transition state of MOR-to-TMP proton transfer was found from any of them (Figure S5). Furthermore, attempts at optimizing a proton transfer product (i.e., an ion pair containing a protonated TMP cation) all converged reversely to the starting **IM6**−TMP complex. These results suggest that the MOR-to-TMP proton transfer would not be feasible. As opposed to coordination to Pd(II), the coordination of MOR to the lower oxidation state Co(I) center cannot increase the acidity of MOR to a point where it can be deprotonated by TMP, a weak organic base. Such is an insight into the nonexistence of the deprotonation pathways. We also considered a third possible inner-sphere mechanism, namely, the concerted σ-bond metathesis between the N−H and Co−C(acyl) bonds in **IM6**, but did not find the envisioned four-membered ring transition state.

We now turn our attention to possible outer-sphere pathways, as a previous kinetics study proposed an outer-sphere attack of a nucleophile (MeOH) on an acylcobalt complex to form an ester product.[26] We have considered the attack of MOR on the acyl group of **IM7** from outside the coordination sphere, as shown in Figure 6. MOR can approach the planar acyl carbon from two different sides via **TS6a** or **TS6b**. **TS6b** is higher in energy than **TS6a** by 3.6 kcal/mol and therefore disfavored. **TS6a** proceeds to the ion pair **IM9**, which contains the product amide in a protonated form. This amide C−N bond-forming step is kinetically facile ($\Delta G^{\ddagger}$ = 14.1 kcal/mol) and thermodynamically downhill (ΔG = −5.1 kcal/mol). **IM9** dissociates to give the protonated amide **IM10** and regenerate **2cat**. The significant increase in the acidity of the ammonium cation **IM10** facilitates its deprotonation by TMP through the hydrogen-bonded complex **IM11** and the transition state **TS7**. Note that **TS7** is higher than **IM11** by 0.1 and 0.2 kcal/mol in electronic energy in the gas phase and in solution, respectively, but becomes lower than **IM11** by 0.8 kcal/mol in free energy after thermal correction. This suggests a facile and essentially barrierless conversion. In addition, the deprotonation process from **IM10** through the final amide product provides the largest driving force (ΔG = −28.7 kcal/mol) for the overall reaction. There is an alternative but less favorable pathway through **IM9** in which **IM9** releases the amide product by the N-to-Co proton transfer (Figure S6).

Apart from the abovementioned inner-sphere mechanism proposed for Pd-catalyzed aminocarbonylation,[25] a computational study by Maseras et al. proposed an amide C−N bond formation via a base (DBU)-assisted outer-sphere attack of NH_3 on a Pd-bound acyl group,[27] where DBU is 1,8-diazabicyclo-[5.4.0]undec-7-ene. We considered a similar mechanism involving the nucleophilic attack of MOR on the acyl group of **IM7** assisted by the base TMP, which turned out to be disfavored (Figure S7). Thus, the pathway shown in Figure 6 represents a new outer-sphere amide C−N bond-forming mechanism established for transition-metal-catalyzed

https://dx.doi.org/10.1021/acscatal.9b04736
ACS Catal. 2020, 10, 1520−1527

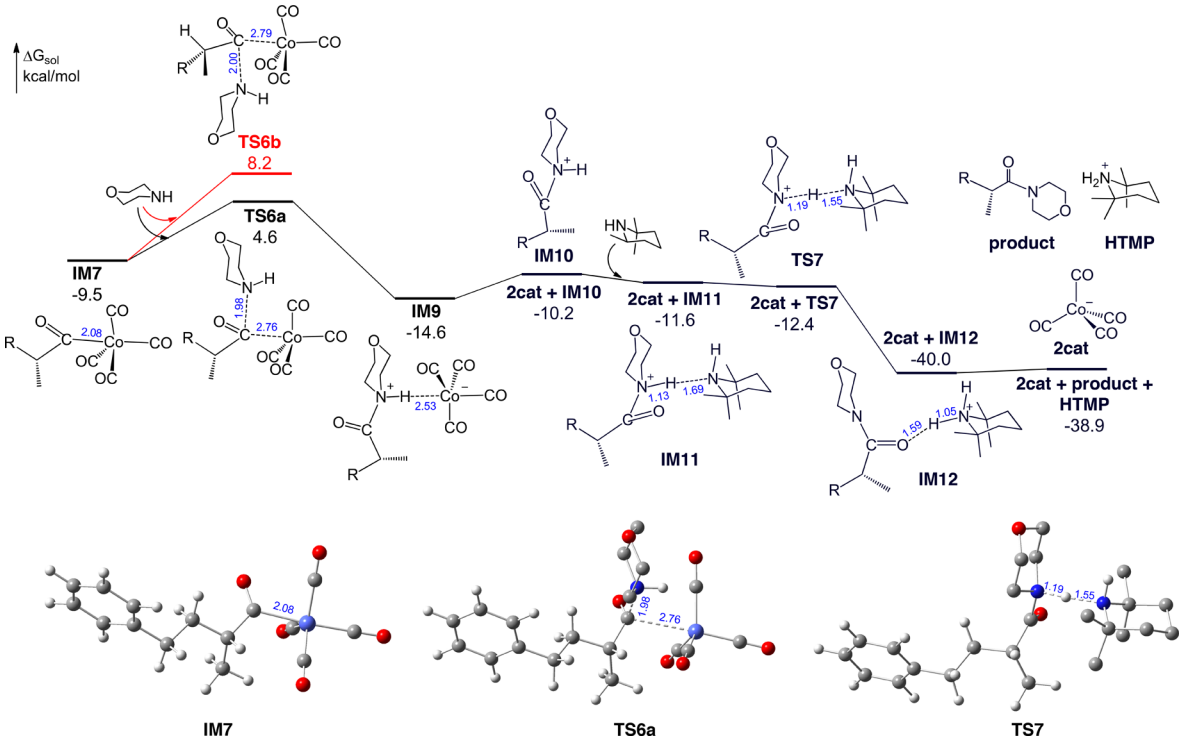

Figure 6. Free-energy profile for the amide C−N bond formation and subsequent deprotonation.

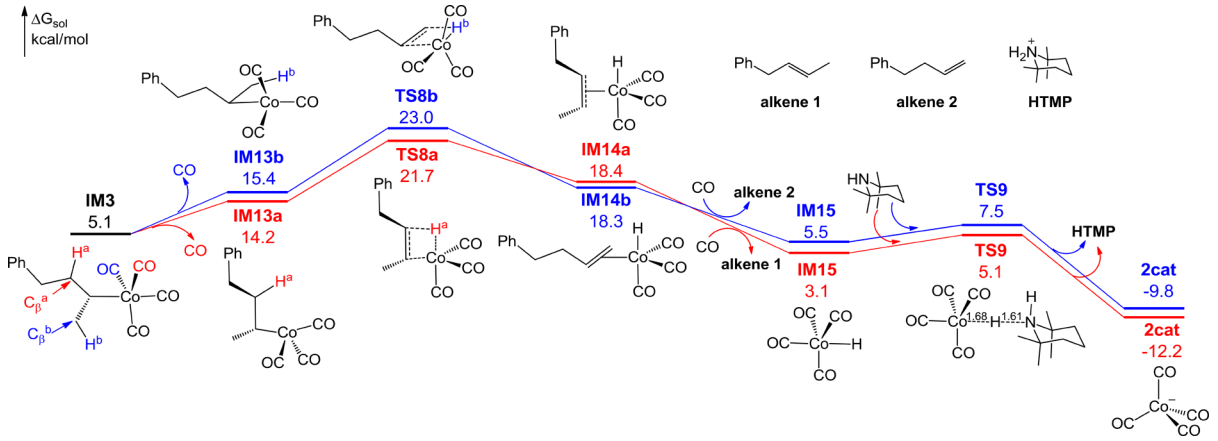

Figure 7. Free-energy profile for the β-hydride elimination pathways.

aminocarbonylation, which does not invoke extra assistance in the nucleophilic attack of amine.

The free-energy surface for the complete reaction pathway beginning with the precatalyst **1cat** has now been mapped out, with every intermediate and transition state molecularly well-defined and energetically reasonable (Figures 3, 4, and 6). The largest energy span[28] is from **2cat** to **TS2** (22.8 kcal/mol). The S_N2 reaction via **TS2** is the rate-determining step.

3.4. Chemoselectivity and Side Reactions. The three-component title reaction generates the amide product in 85% yield when competing reactions are also possible. To rationalize the high chemoselectivity, we studied the free-energy profiles for two possible side reactions: β-hydride elimination and double CO insertion.

As shown in Figure 7, the Co(I) alkyl intermediate **IM3** can undertake β-hydride elimination to give alkene products. There are two groups of β-hydrogen atoms in **IM3**, and for each group, we located the lowest energy β-hydride elimination transition state **TS8a**/**TS8b**. The β-H^a/β-H^b elimination proceeds via **TS8a**/**TS8b** to **IM15** and delivers **alkene 1**/**alkene 2**. **IM15** can be deprotonated by TMP via **TS9** to regenerate **2cat**. These β-hydride elimination pathways are thermodynamically feasible (ΔG = −9.8 or − 12.2 kcal/mol), but they are kinetically much less favorable than the CO insertion pathway through **TS3** (Figure 4). **TS8a**, the lowest β-hydride elimination barrier, is 9.8 kcal/mol higher than **TS3** in energy, and the barriers after **TS3** in the main reaction pathway are all lower than **TS3** (Figures 4 and 6). Therefore, there is an overwhelming preference for CO insertion over β-hydride elimination at **IM3**. The difference of 9.8 kcal/mol in energy between **TS8a** and **TS3** mostly stems from the endergonic conversion **IM3** → **IM13a** (ΔG = 9.1 kcal/mol) in which a CO ligand dissociates from the 18-electron **IM3** to vacate a coordination site for the ensuing β-hydride elimination (Figure 7). By contrast, the CO insertion via **TS3** takes place directly from **IM3** (Figure 4).

https://dx.doi.org/10.1021/acscatal.9b04736
ACS Catal. 2020, 10, 1520−1527

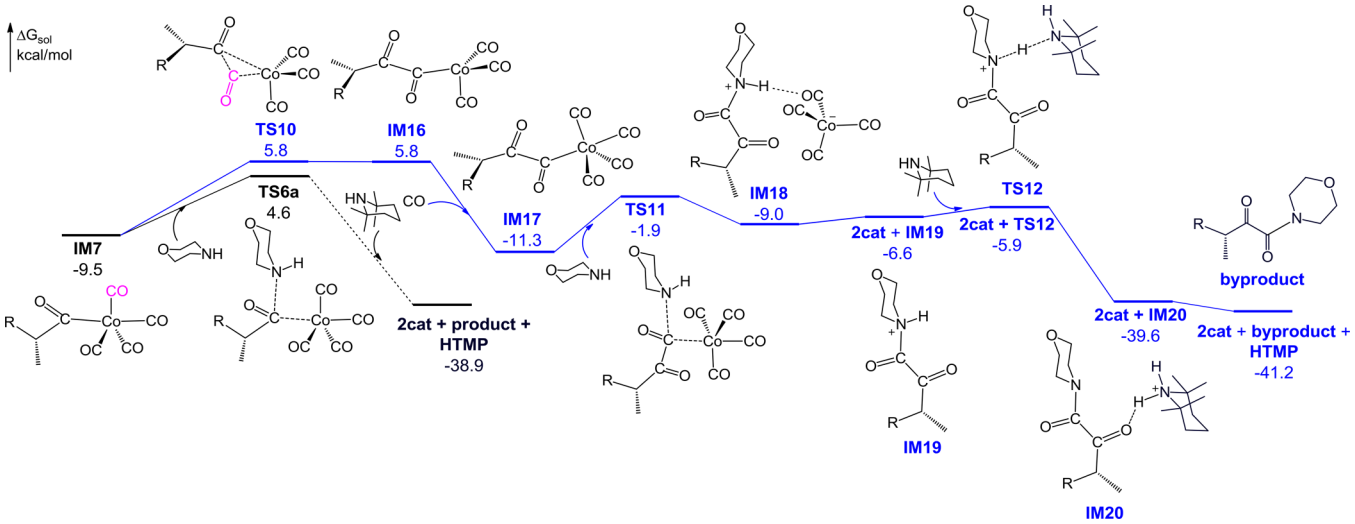

Figure 8. Free-energy profile for the double CO insertion pathway compared with the main reaction pathway through TS6a (see Figure 6 for the full representation).

As shown in Figure 8, the Co(I) acyl intermediate **IM7** can undertake intramolecular CO insertion via **TS10**, followed by external CO coordination, to form the 18-electron intermediate **IM17**. This biacetyl species, upon an outer-sphere nucleophilic attack by MOR, proceeds via **TS11** to give the ion pair **IM18**, which contains the byproduct amide in a protonated form. Dissociation of **IM18**, followed by deprotonation by TMP via **TS12**, leads to the final byproduct amide. This competing reaction pathway and the pathway leading to the major product are branches from **IM7**, which respectively have **TS10** and **TS6a** as the highest points in energy (Figure 8). Therefore, **TS6a** and **TS10** are the selectivity-determining energy barriers, the former being lower than the latter by 1.2 kcal/mol. This difference in energy suggests that single CO insertion is favored over double CO insertion.

4. CONCLUSIONS

We have utilized DFT calculations to establish a detailed mechanism for the cobalt-catalyzed chemoselective aminocarbonylation of unactivated alkyl electrophiles. Morpholine, the amine substrate, induces the disproportionation of $Co_2(CO)_8$ to form $[Co(CO)_4]^-$. This active species undergoes an S_N2 reaction with the alkyl electrophile via **TS2** to form the alkylcobalt(I) carbonyl intermediate **IM3**, which favors CO migratory insertion over β-hydride elimination. The CO insertion generates an acylcobalt(I) carbonyl intermediate from which point the reaction could follow several amide C−N bond-forming pathways. The inner-sphere pathways have been ruled out because of the extremely high energy barriers. The outer-sphere pathway in which morpholine attacks the Co(I)-bound acyl group via **TS6a** has been established. The overall reaction is energetically downhill, with the S_N2 process via **TS2** being the rate-determining step ($\Delta G^{\ddagger}$ = 22.8 kcal/mol). The stereospecificity of the reaction originates from the Walden inversion in the S_N2 step. The side reaction of double CO insertion is kinetically less favorable.

The computational results demonstrate rich experimental−theoretical synergy and provide deep insights into how the common cobalt reagent $Co_2(CO)_8$ promotes the three-component chemoselective aminocarbonylation of unactivated alkyl electrophiles, which can have implications for organocobalt catalysis and transition-metal-enabled amide C−N bond-forming reactions.

■ ASSOCIATED CONTENT

Supporting Information

The Supporting Information is available free of charge at https://pubs.acs.org/doi/10.1021/acscatal.9b04736.

Additional computational results and energies and Cartesian coordinates of the optimized structures (PDF)

■ AUTHOR INFORMATION

Corresponding Author

Xiaotai Wang − *Shenzhen Polytechnic, Shenzhen, P. R. China, and University of Colorado Denver, Denver, Colorado;* orcid.org/0000-0003-3310-3308; Email: xiaotai.wang@ucdenver.edu

Other Authors

Jiandong Guo − *Shenzhen Polytechnic, Shenzhen, P. R. China, and Shandong University, Jinan, P. R. China*

Hai D. Pham − *University of Colorado Denver, Denver, Colorado*

Yan-Bo Wu − *Shanxi University, Taiyuan, P. R. China;* orcid.org/0000-0001-6032-9957

Dongju Zhang − *Shandong University, Jinan, P. R. China*

Complete contact information is available at: https://pubs.acs.org/10.1021/acscatal.9b04736

Notes

The authors declare no competing financial interest.

■ ACKNOWLEDGMENTS

We acknowledge support for this work from the Hoffmann Institute of Advanced Materials, Shenzhen Polytechnic and the University of Colorado Denver. D.Z. acknowledges support from the National Natural Science Foundation of China (grant no. 21773139). We thank the anonymous reviewers for their insightful and helpful comments.

https://dx.doi.org/10.1021/acscatal.9b04736
ACS Catal. 2020, 10, 1520−1527

REFERENCES

(1) Pattabiraman, V. R.; Bode, J. W. Rethinking amide bond synthesis. *Nature* **2011**, *480*, 471−479.

(2) Schoenberg, A.; Heck, R. F. Palladium-catalyzed amidation of aryl, heterocyclic, and vinylic halides. *J. Org. Chem.* **1974**, *39*, 3327−3331.

(3) (a) Atkins, R. J.; Banks, A.; Bellingham, R. K.; Breen, G. F.; Carey, J. S.; Etridge, S. K.; Hayes, J. F.; Hussain, N.; Morgan, D. O.; Oxley, P.; Passey, S. C.; Walsgrove, T. C.; Wells, A. S. The Development of a Manufacturing Route for the GPIIb/IIIa Receptor Antagonist SB-214857-A. Part 2: Conversion of the Key Intermediate SB-235349 to SB-214857-A. *Org. Process Res. Dev.* **2003**, *7*, 663−675. (b) Brennführer, A.; Neumann, H.; Beller, M. Palladium-catalyzed carbonylation reactions of aryl halides and related compounds. *Angew. Chem., Int. Ed.* **2009**, *48*, 4114−4133. (c) Wu, X.-F.; Neumann, H.; Beller, M. Selective Palladium-Catalyzed Aminocarbonylation of Aryl Halides with CO and Ammonia. *Chem. − Eur. J.* **2010**, *16*, 9750−9753. (d) Martinelli, J. R.; Freckmann, D. M. M.; Buchwald, S. L. Convenient Method for the Preparation of Weinreb Amides via Pd-Catalyzed Aminocarbonylation of Aryl Bromides at Atmospheric Pressure. *Org. Lett.* **2006**, *8*, 4843−4846. (e) Martinelli, J. R.; Clark, T. P.; Watson, D. A.; Munday, R. H.; Buchwald, S. L. Palladium-Catalyzed Aminocarbonylation of Aryl Chlorides at Atmospheric Pressure: The Dual Role of Sodium Phenoxide. *Angew. Chem., Int. Ed.* **2007**, *46*, 8460−8463. (f) Friis, S. D.; Skrydstrup, T.; Buchwald, S. L. Mild Pd-Catalyzed Aminocarbonylation of (Hetero)Aryl Bromides with a Palladacycle Precatalyst. *Org. Lett.* **2014**, *16*, 4296−4299.

(4) (a) Urata, H.; Ishii, Y.; Fuchikami, T. Palladium-catalyzed double carbonylation of alkyl iodides bearing perfluoroalkyl group. *Tetrahedron Lett.* **1989**, *30*, 4407−4410. (b) Fukuyama, T.; Nishitani, S.; Inouye, T.; Morimoto, K.; Ryu, I. Effective Acceleration of Atom Transfer Carbonylation of Alkyl Iodides by Metal Complexes. Application to the Synthesis of the Hinokinin Precursor and Dihydrocapsaicin. *Org. Lett.* **2006**, *8*, 1383−1386. (c) Fukuyama, T.; Inouye, T.; Ryu, I. Atom transfer carbonylation using ionic liquids as reaction media. *J. Organomet. Chem.* **2007**, *692*, 685−690. (d) Rahman, O.; Långström, B.; Halldin, C. Alkyl Iodides and [^{11}C] CO in Nickel-Mediated Cross-Coupling Reactions: Successful Use of Alkyl Electrophiles containing a β Hydrogen Atom in Metal-Mediated [^{11}C] Carbonylation. *ChemistrySelect* **2016**, *1*, 2498−2501.

(5) Sargent, B. T.; Alexanian, E. J. Cobalt-Catalyzed Aminocarbonylation of Alkyl Tosylates: Stereospecific Synthesis of Amides. *Angew. Chem., Int. Ed.* **2019**, *58*, 9533−9536.

(6) Frisch, M. J.; Trucks, G. W.; Schlegel, H. B.; Scuseria, G. E.; Robb, M. A.; Cheeseman, J. R.; Scalmani, G.; Barone, V.; Men-nucci, B.; Petersson, G. A.; Nakatsuji, H.; Caricato, M.; Li, X.; Hratchian, H. P.; Izmaylov, A. F.; Bloino, J.; Zheng, G.; Sonnen-berg, J. L.; Hada, M.; Ehara, M.; Toyota, K.; Fukuda, R.; Hasegawa, J.; Ishida, M.; Nakajima, T.; Honda, Y.; Kitao, O.; Nakai, H.; Vreven, T.; Montgomery, J. A., Jr.; Peralta, J. E.; Ogliaro, F.; Bearpark, M.; Heyd, J. J.; Brothers, E.; Kudin, K. N.; Staroverov, V. N.; Kobayashi, R.; Normand, J.; Raghavachari, K.; Rendell, A.; Burant, J. C.; Iyengar, S. S.; Tomasi, J.; Cossi, M.; Rega, N.; Millam, J. M.; Klene, M.; Knox, J. E.; Cross, J. B.; Bakken, V.; Adamo, C.; Jaramillo, J.; Gomperts, R.; Stratmann, R. E.; Yazyev, O.; Austin, A. J.; Cammi, R.; Pomelli, C.; Ochterski, J. W.; Martin, R. L.; Morokuma, K.; Zakrzewski, V. G.; Voth, G. A.; Salvador, P.; Dannenberg, J. J.; Dapprich, S.; Daniels, A. D.; Farkas, O.; Foresman, J. B.; Ortiz, J. V.; Cioslowski, J.; Fox, D. J. *Gaussian 09*, revision D.01; Gaussian Inc.: Wallingford, CT, 2013.

(7) (a) Lee, C.; Yang, W.; Parr, R. G. Development of the Colle-Salvetti Correlation-Energy Formula into a Functional of the Electron Density. *Phys. Rev. B* **1988**, *37*, 785−789. (b) Becke, A. D. A new mixing of Hartree-Fock and local density-functional theories. *J. Chem. Phys.* **1993**, *98*, 1372−1377. (c) Becke, A. D. Density-F unctional Thermochemistry. III. The Role of Exact Exchange. *J. Chem. Phys.* **1993**, *98*, 5648−5652. (d) Stephens, P. J.; Devlin, F. J.; Chabalowski, C. F.; Frisch, M. J. Ab Initio Calculation of Vibrational Absorption and Circular Dichroism Spectra Using Density Functional Force Fields. *J. Phys. Chem.* **1994**, *98*, 11623−11627.

(8) Grimme, S.; Antony, J.; Ehrlich, S.; Krieg, H. A consistent and accurate ab initio parametrization of density functional dispersion correction (DFT-D) for the 94 elements H−Pu. *J. Chem. Phys.* **2010**, *132*, 154104−154119.

(9) (a) Andrae, D.; Häußermann, U.; Dolg, M.; Stoll, H.; Preuß, H. Energy-Adjusted *ab* initio Pseudopotentials for the Second and Third Row Transition Elements. *Theor. Chim. Acta* **1990**, *77*, 123−141. (b) Dolg, M.; Wedig, U.; Stoll, H.; Preuss, H. Energy-Adjusted ab initio Pseudopotentials for the First Row Transition Elements. *J. Chem. Phys.* **1987**, *86*, 866−872.

(10) Marenich, A. V.; Cramer, C. J.; Truhlar, D. G. Universal Solvation Model Based on Solute Electron Density and on a Continuum Model of the Solvent Defined by the Bulk Dielectric Constant and Atomic Surface Tensions. *J. Phys. Chem. B* **2009**, *113*, 6378−6396.

(11) *t*-Amyl alcohol is not among the solvents that Gaussian 09 predefined for the SMD model, so the closest predefined solvent *t*-butyl alcohol was used instead.

(12) (a) Benson, S. W. *The Foundations of Chemical Kinetics*; R. E. Krieger: Malabar, FL, 1982. (b) Schoenebeck, F.; Houk, K. N. Ligand-Controlled Regioselectivity in Palladium-Catalyzed Cross Coupling Reactions. *J. Am. Chem. Soc.* **2010**, *132*, 2496−2497. (c) Liu, B.; Gao, M.; Dang, L.; Zhao, H.; Marder, T. B.; Lin, Z. DFT Studies on the Mechanisms of the Platinum-Catalyzed Diboration of Acyclic α, β-Unsaturated Carbonyl Compounds. *Organometallics* **2012**, *31*, 3410−3425. (d) Zhou, Q.; Li, Y. The Real Role of N-Heterocyclic Carbene in Reductive Functionalization of CO_2: An Alternative Understanding from Density Functional Theory Study. *J. Am. Chem. Soc.* **2015**, *137*, 10182−10189.

(13) (a) Pino, P.; Piacenti, F.; Bianchi, M. *Organic Synthesis via Metal Carbonyls*; Wender, I.; Pino, P., Eds.; Wiley: New York, 1977; Vol. *2*, pp 43−231. (b) Pruett, R. L. Hydroformylation. *Adv. Organomet. Chem.* **1979**, *17*, 1−60. (c) Beller, M.; Cornils, B.; Frohning, C. D.; Kohlpaintner, C. W. Progress in hydroformylation and carbonylation. *J. Mol. Catal. A: Chem.* **1995**, *104*, 17−85. (d) Dwyer, C.; Assumption, H.; Coetzee, J.; Crause, C.; Damoense, L.; Kirk, M. Hydroformylation studies using high pressure NMR spectroscopy. *Coord. Chem. Rev.* **2004**, *248*, 653−669. (e) Hebrard, F.; Kalck, P. Cobalt-Catalyzed Hydroformylation of Alkenes: Generation and Recycling of the Carbonyl Species, and Catalytic Cycle. *Chem. Rev.* **2009**, *109*, 4272−4282. (f) Bungu, P. N.; Otto, S. Evaluation of ligand effects in the modified cobalt hydroformylation of 1-octene. Crystal structures of $[Co(L)(CO)_3]_2$ (L = PA−C_5, PCy_3 and $PCyp_3$). *Dalton Trans.* **2011**, *40*, 9238−9249.

(14) (a) Brummond, K. M.; Kent, J. L. Recent Advances in the Pauson−Khand Reaction and Related [2+2+1] Cycloadditions. *Tetrahedron* **2000**, *56*, 3263−3283. (b) Blanco-Urgoiti, J.; Añorbe, L.; Pérez-Serrano, L.; Domínguez, G.; Pérez-Castells, J. The Pauson−Khand reaction, a powerful synthetic tool for the synthesis of complex molecules. *Chem. Soc. Rev.* **2004**, *33*, 32−42. (c) Lee, H.-W.; Kwong, F.-Y. A Decade of Advancements in Pauson−Khand-Type Reactions. *Eur. J. Org. Chem.* **2010**, *2010*, 789−811.

(15) (a) Harrod, J. F.; Chalk, A. J. Dicobalt Octacarbonyl as a Catalyst for Hydrosilation of Olefins. *J. Am. Chem. Soc.* **1965**, *87*, 1133−1133. (b) Crivello, J. V.; Rajaraman, S. K. Dicobalt octacarbonyl-catalyzed tandem isomerization and cationic polymerization of functionalized allylic ethers. *J. Polym. Sci., Part A: Polym. Chem.* **1999**, *37*, 687−690. (c) Son, S. U.; Choi, D. S.; Chung, Y. K.; Lee, S.-G. Dicobalt Octacarbonyl-Catalyzed Tandem [2 + 2 + 1] and [2 + 2 + 2] Cycloaddition Reaction of Diynes with Two Phenylacetylenes under CO. *Org. Lett.* **2000**, *2*, 2097−2100. (d) Shibata, T.; Yamashita, K.; Takagi, K.; Ohta, T.; Soai, K. Inter- and Intramolecular Carbonylative Alkyne−Alkyne Coupling Reaction Mediated by Cobalt Carbonyl Complex. *Tetrahedron* **2000**, *56*, 9259−9267.

(16) (a) Bor, G.; Noack, K. On the infrared spectrum of dicobalt octacarbonyl. Results of ^{13}co enrichment studies. *J. Organomet. Chem.* **1974**, *64*, 367−372. (b) Onaka, S.; Shriver, D. F. Application of Raman spectroscopy to bridged-nonbridged equilibria for polynuclear

https://dx.doi.org/10.1021/acscatal.9b04736
ACS Catal. 2020, 10, 1520−1527

metal carbonyl derivatives. Metal-metal stretching frequencies of octacarbonyldicobalt, octacarbonyldiferrate(2-), dodecacarbonyltetracobalt, and bis[.eta.-cyclopentadienyl)dicarbonylruthenium]. *Inorg. Chem.* **1976**, *15*, 915−918. (c) Bor, G.; Dietler, U. K.; Noack, K. High temperature infrared spectrum of dicobalt octacarbonyl: predominance of the third isomer. *J. Chem. Soc., Chem. Commun* **1976**, 914−916. (d) Sweany, R. L.; Brown, T. L. Infrared spectra of matrix-isolated dicobalt octacarbonyl. Evidence for the third isomer. *Inorg. Chem.* **1977**, *16*, 415−421.

(17) (a) Aullón, G.; Alvarez, S. The $[M_2(CO)_8]$ Complexes of the Cobalt Group. *Eur. J. Inorg. Chem.* **2001**, *2001*, 3031−3038. (b) Macchi, P.; Garlaschelli, L.; Sironi, A. Electron Density of Semi-Bridging Carbonyls. Metamorphosis of CO Ligands Observed via Experimental and Theoretical Investigations on $[FeCo(CO)_8]^-$. *J. Am. Chem. Soc.* **2002**, *124*, 14173−14184.

(18) (a) Hieber, W.; Freyer, W. Zur Kenntnis der Reaktionen des Kobalttetracarbonyls mit verschiedenartigen Basen, VII. Reaktionen des Kobaltcarbonyls mit Verbindungen des 3-wertigen Phosphors und seiner Homologen. *Chem. Ber.* **1960**, *93*, 462−467. (b) Attali, S.; Poilblanc, R. Trivalent phosphorus derivatives of cobalt carbonyls. II. Synthesis and physico-chemical studies of new cations in the hypothetical pentacarbonyl cobalt(I) series. *Inorg. Chim. Acta* **1972**, *6*, 475−479. (c) van Rensburg, H.; Tooze, R. P.; Foster, D. F.; Otto, S. Synthesis and Characterization of a Novel Cobalt Carbonyl N-Heterocyclic Carbene Salt. Crystal Structure of $[Co(CO)_3(IMes)_2]^+[Co(CO)_4]^-$. *Inorg. Chem.* **2007**, *46*, 1963−1965.

(19) Bondi, A. van der Waals Volumes and Radii. *J. Phys. Chem.* **1964**, *68*, 441−451.

(20) (a) Batsanov, S. S. Van der Waals radii of elements. *Russ. J. Inorg. Chem.* **1991**, *36*, 1694−1706. (b) Batsanov, S. S. Van der Waals radii of elements. *Inorg. Mater.* **2001**, *37*, 871−885.

(21) Hegedus, L. S.; Inoue, Y. Cobalt-mediated 1,4-acylation/alkylation of 1,3-dienes. *J. Am. Chem. Soc.* **1982**, *104*, 4917−4921.

(22) (a) Musaev, D. G.; Morokuma, K. Ab Initio Molecular Orbital Study of the Mechanism of H−H, C−H, N−H, O−H and Si−H Bond Activation on Transient Cyclopentadienylcarbonylrhodium. *J. Am. Chem. Soc.* **1995**, *117*, 799−805. (b) Vélez, E.; Betoré, M. P.; Casado, M. A.; Polo, V. N−H Activation of Ammonia by $[\{M(\mu\text{-}OMe)(cod)\}_2]$ (M = Ir, Rh) Complexes: A DFT Study. *Organometallics* **2015**, *34*, 3959−3966.

(23) (a) Blomberg, M. R. A.; Siegbahn, P. E. M.; Svensson, M. Theoretical study of the activation of the nitrogen−hydrogen bond in ammonia by second row transition metal atoms. *Inorg. Chem.* **1993**, *32*, 4218−4225. (b) Sykes, A. C.; White, P.; Brookhart, M. Reactions of Anilines and Benzamides with a 14-Electron Iridium(I) Bis(phosphinite) Complex: N−H Oxidative Addition versus Lewis Base Coordination. *Organometallics* **2006**, *25*, 1664−1675.

(24) Sunesson, Y.; Limé, E.; Nilsson Lill, S. O.; Meadows, R. E.; Norrby, P.-O. Role of the Base in Buchwald−Hartwig Amination. *J. Org. Chem.* **2014**, *79*, 11961−11969.

(25) (a) Wang, J. Y.; Strom, A. E.; Hartwig, J. F. Mechanistic Studies of Palladium-Catalyzed Aminocarbonylation of Aryl Chlorides with Carbon Monoxide and Ammonia. *J. Am. Chem. Soc.* **2018**, *140*, 7979−7993. (b) Wang, Q.; Huang, F.; Liu, J.; Wang, W.; Sun, C.; Chen, D. Ligands and Bases Mediate Switching between Aminocarbonylations and Alkoxycarbonylations in Coupling of Aminophenols with Iodoarenes. *Inorg. Chem.* **2019**, *58*, 10217−10226. (c) Liu, Y.; Zhang, Z.; Zhang, S.; Zhang, Y.; Wang, J.; Zhang, Z. Pd^0-Catalyzed Four-Component Reaction of Aryl Halide, CO, N-Tosylhydrazone, and Amine. *Chem. − Asian J.* **2018**, *13*, 3658−3663.

(26) Sóvágó, J.; Sisak, A.; Ungváry, F.; Markó, L. Kinetics and mechanism of the methanolysis of acetylcobalt tetracarbonyl. *Inorg. Chim. Acta* **1994**, *227*, 297−300.

(27) Fernández-Alvarez, V. M.; de la Fuente, V.; Godard, C.; Castillón, S.; Claver, C.; Maseras, F.; Carbó, J. J. Pd-Catalysed Mono- and Dicarbonylation of Aryl Iodides: Insights into the Mechanism and the Selectivity. *Chem. − Eur. J.* **2014**, *20*, 10982−10989.

(28) (a) Kozuch, S.; Shaik, S. A combined kinetic−quantum mechanical model for assessment of catalytic cycles: Application to cross-coupling and Heck reactions. *J. Am. Chem. Soc.* **2006**, *128*, 3355−3365. (b) Kozuch, S.; Shaik, S. How to Conceptualize Catalytic Cycles? The Energetic Span Model. *Acc. Chem. Res.* **2011**, *44*, 101−110.

https://dx.doi.org/10.1021/acscatal.9b04736
ACS Catal. 2020, 10, 1520−1527